

Dislocation based controlling of kinematic hardening contribution to simulate primary and secondary stages of uniaxial ratcheting

S Bhattacharjee¹, S Dhar^{1,*} and S K Acharyya¹

¹Jadavpur University, Kolkata, West Bengal, India, 700032

* Corresponding Author e-mail: sankar_dhar1@rediffmail.com, Telefax: +91 33 2414 6532

Abstract: The primary and secondary stages of the uniaxial ratcheting curve for the C-Mn steel SA333 have been investigated. Stress controlled uniaxial ratcheting experiments were conducted with different mean stresses and stress amplitudes to obtain curves showing the evolution of ratcheting strain with number of cycles. In stage-I of the ratcheting curve, a large accumulation of ratcheting strain occurs, but at a decreasing rate. In contrast, in stage-II a smaller accumulation of ratcheting strain is found and the ratcheting rate becomes almost constant. Transmission electron microscope observations reveal that no specific dislocation structures are developed during the early stages of ratcheting. Rather, compared with the case of low cycle fatigue, it is observed that sub-cell formation is delayed in the case of ratcheting. The increase in dislocation density as a result of the ratcheting strain is obtained using the Orowan equation. The ratcheting strain is obtained from the shift of the plastic strain memory surface. The dislocation rearrangement is incorporated in a functional form of dislocation density, which is used to calibrate the parameters of a kinematic hardening law. The observations are formulated in a material model, plugged into the ABAQUS finite element (FE) platform as a user material subroutine. Finally the FE-simulated ratcheting curves are compared with the experimental curves.

1. Introduction

Cyclic plastic deformation occurs when a material is subjected to an load with an amplitude beyond its yield limit. The experimental results form the framework of the material response under different cyclic loading conditions. When it comes to modeling of the cyclic plastic behavior, a key role is played by the kinematic hardening (KH) rule, to generate the cyclic hysteresis loops and to describe fundamental cyclic plastic phenomena such as the Bauschinger effect. There are other different material responses observed for balanced cyclic loading, in which cyclic hardening or softening behavior is observed experimentally.

During low cycle fatigue, dislocation substructures are formed surrounded by low angle sub-grain boundaries containing arrays of trapped edge dislocations [1]. Dislocation annihilations are likely to occur when moving dislocations interact with low angle subgrain boundaries. The annihilation of boundary dislocations can be a reasonable phenomenon to justify isotropic cyclic softening in low cycle fatigue (LCF) loadings [2].

On the other hand, when a material is subjected to unbalanced cyclic loading, a ratcheting phenomenon is observed, as the accumulation of plastic strain in loading direction. Transmission



electron microscope (TEM) observations show that the formation of a substructure during asymmetric loading is difficult and generally delayed, due to the continuous generation of new dislocations triggered by the asymmetry in loading. Potentially, these new dislocations can pile-up and increase the hardening [3,4].

In this work, the isotropic softening phenomenon based on dislocation annihilation at low angle tilt boundaries is employed for the simulation of cyclic softening behavior. The Ohno-Wang kinematic hardening rule [5] is employed to simulate basic stress-strain hysteresis loops including a Bauschinger effect. For asymmetric loading, the extra hardening evolves due to the generation of an excess dislocation density corresponding to the ratcheting strain. The KH parameters of the Ohno-Wang law are calibrated with an appropriate dislocation function to incorporate this extra hardening. The developed material model is plugged into the ABAQUS CAE (v6.8) commercial finite element software in the form of a user defined material subroutine (UMAT) and the simulated results are compared with the experimental data.

2. Material

SA333 Grade-6 C-Mn steel is commonly used in primary heat transport pipes in Indian PHWR nuclear power plants. The chemical composition of SA333 Grade-6 C-Mn steel is shown in table 1.

Table 1. Chemical composition of SA333 C-Mn steel.

Element	C	Mn	Si	P	Fe
wt. (%)	0.18	0.90	0.02	0.02	Rest

The typical microstructure of the material is given in figure 1, showing pearlite bands (volume fraction 30%) in a ferrite matrix with an average ferrite grain size of 22 μ m. It is assumed in the following that all the deformation occurs mainly in the ferrite grains, because ferrite is softer and thus more susceptible to deformation than pearlite.

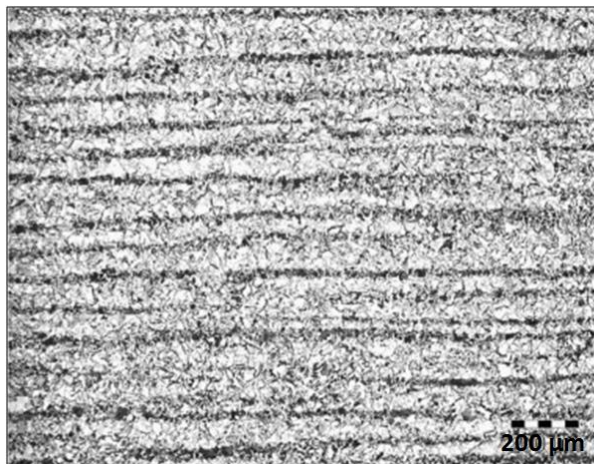


Figure 1. Optical micrograph of SA333.

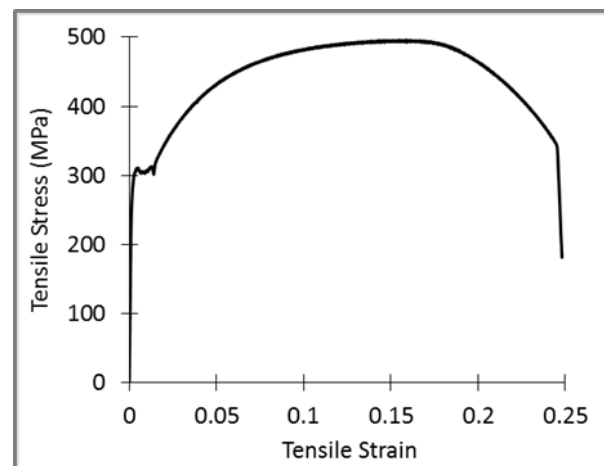


Figure 2. Tensile plot for SA333.

A typical tensile plot of the SA333 is presented in figure 2. The steel has moderate strength ($Y_S = 304$ MPa, $UTS = 495$ MPa) with elastic modulus of 207GPa, and a ductility (elongation) of 24.5%. It is important to note that during tensile testing the material developed large Lüders bands up to about 1.4% strain.

TEM images obtained using a Philips CM200 operated at 200kV are displayed in figure 3 for the material in the as received condition, as well as after a few cycles (10 cycles) and after failure of the samples.

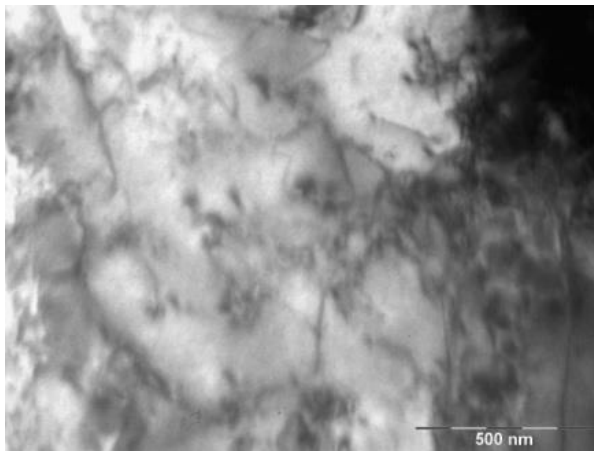


Figure 3a. TEM micrograph of SA333 in the 'as received' condition.

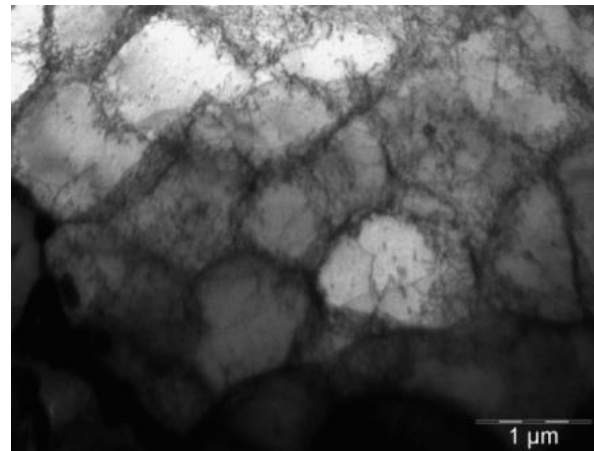


Figure 3b. TEM micrograph of SA333 after 10 cycles (1% strain amplitude).

Although the TEM micrographs of the material in the as received condition (figure 3a) show no definitive dislocation structure, there are nevertheless weak traces of dislocation structures formed during previous plastic deformation.

In contrast, the TEM micrographs of the sample loaded to 10 cycles (figure 3b), show direct evidence for the formation of dislocation substructures. Annihilations of the entrapped dislocations in low angle sub-grain boundaries will result in an isotropic softening stress (negative) and therefore, reduce the cyclic yield stress. Similarly, TEM micrographs of the sample after failure due to balanced cyclic loading (figure 3c) shows the presence of well-defined dislocation substructures, with an average cell size of 1.2 μm.

As a comparison, material subjected to asymmetric loading (mean stress 80MPa; stress amplitude 310MPa) shows delayed formation of a dislocation cell substructure as seen from the TEM micrographs in figure 4a-c. In this unbalanced loading condition, even at half of the lifetime to failure (500 cycles) no distinct sub structure is formed (figure 4a). Continuous generation of new dislocations leads to a bias in the dislocation interactions and entangling behavior is observed. Eventually however the generation rate of new dislocations gradually decreases and a sub-cell dislocation structure is formed (figure 4b).

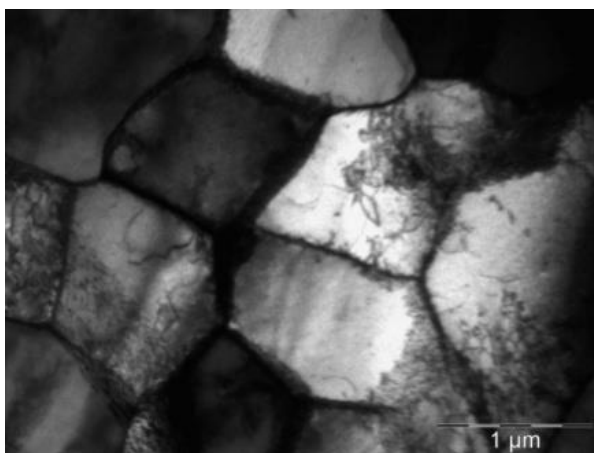


Figure 3c. TEM micrograph of SA333 after failure (1% strain amplitude, 500 cycles).

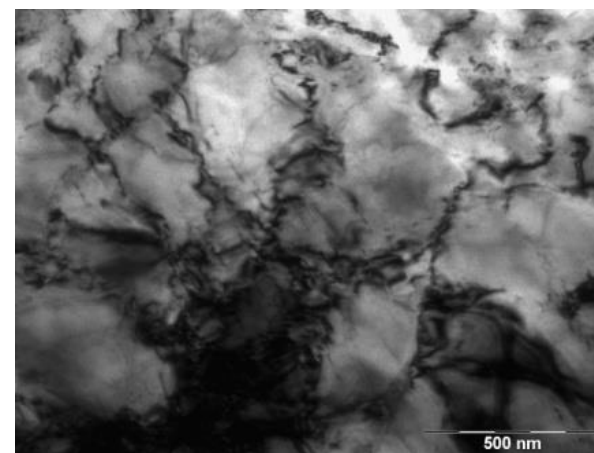


Figure 4a. TEM micrograph of SA333 after half lifetime (≈500 cycles).

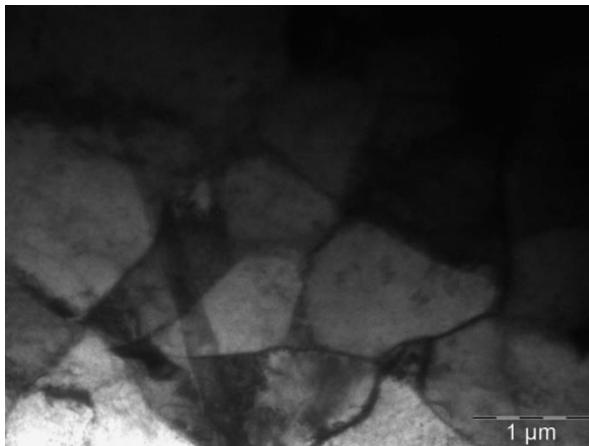


Figure 4b. TEM micrograph of SA333 after failure (longitudinal section of the specimen).

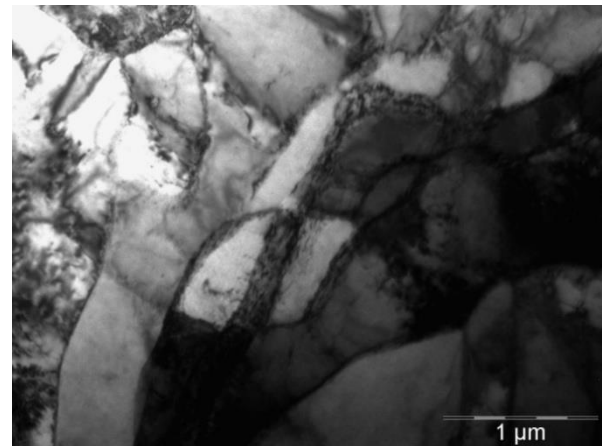


Figure 4c. TEM micrograph of SA333 after failure (cross section of the specimen).

3. Experiments

3.1. Uniaxial LCF experiment

Uniaxial low cycle fatigue tests were conducted by Bhabha Atomic Research Centre, India, at various strain amplitudes ranging from $\pm 0.35\%$ to $\pm 0.75\%$. Typical cyclic plastic phenomena are observed in the stress-strain loops including a Bauschinger effect (figure 5a) and cyclic softening (figure 5b). The cyclic softening rate typically decreases with the number of cycles and saturates within the first 200 cycles. Properties of cyclic hardening/softening depend not only on material microstructure, but also on loading amplitude and more generally on the previous strain history. Such transient behavior of material requires accurate calibration of material parameters.

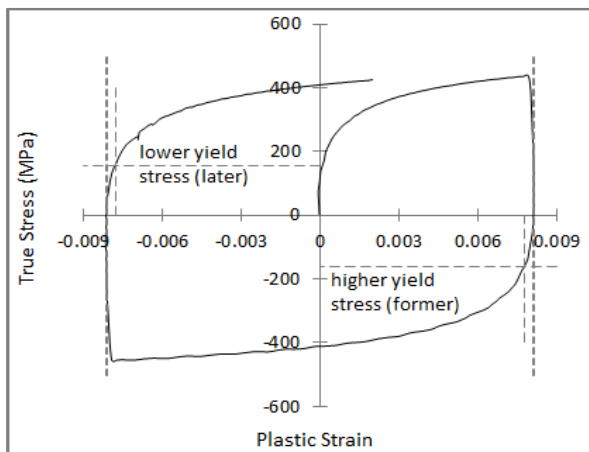


Figure 5a. Experimental results showing Bauschinger effect (0.75% strain amplitude).

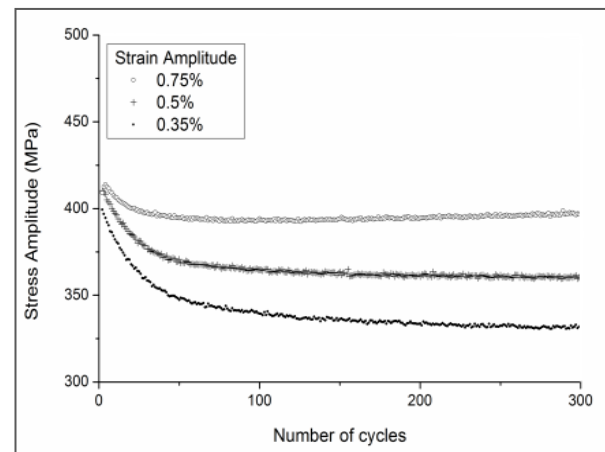


Figure 5b. Experimental results showing cyclic softening (strain amplitude 0.35% to 0.75%).

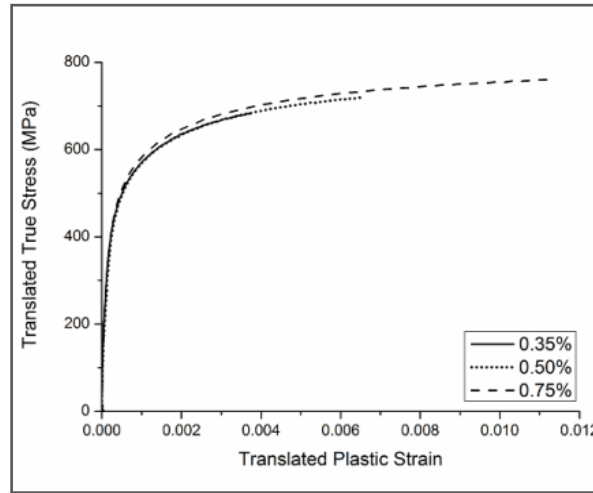


Figure 5c. Experimental results of SA333 showing Masing behavior.

3.2. Uniaxial Ratcheting tests

The evolution of the engineering ratcheting strain [given as $(\epsilon_{\max} + \epsilon_{\min})/2$] as a function of number of cycles during engineering stress-controlled experiments are shown in figure 6a-b for stress amplitudes of 310MPa, 350MPa and 390MPa and mean stresses of 40MPa, 80MPa, and 120MPa. It is observed that significant amounts of ratcheting strain are accumulated before failure.

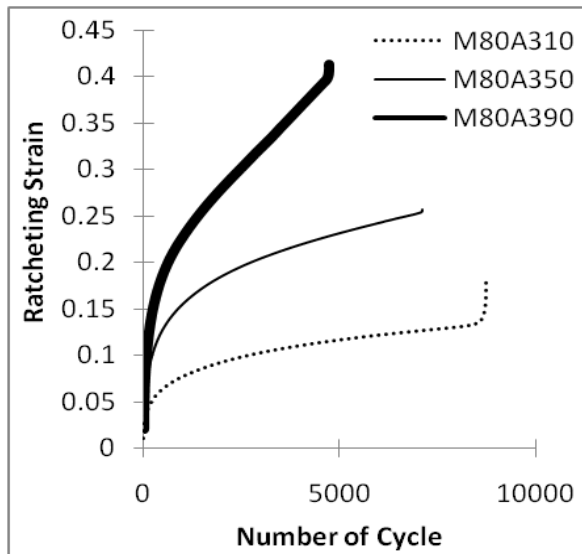


Figure 6a. Stress controlled ratcheting of SA333 showing a comparison between stress amplitudes of 310MPa, 350MPa and 390MPa (all with mean stress of 80MPa).

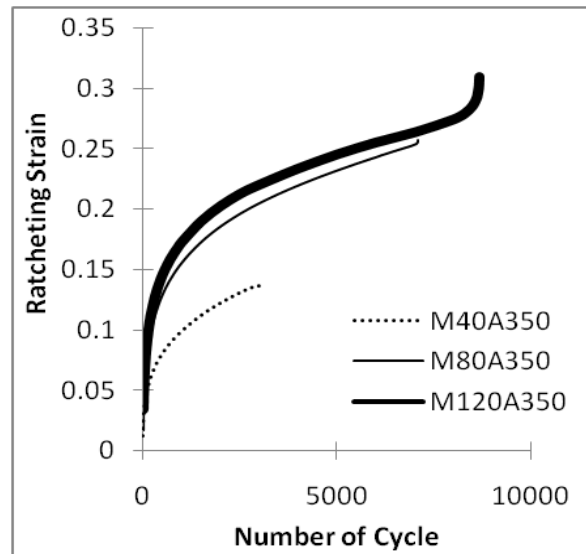


Figure 6b. Stress controlled ratcheting for SA333 Showing a comparison between mean stresses of 40MPa, 80MPa and 120MPa (for a stress amplitude of 350MPa).

4. Material model

In order to model material plasticity a suitable yield criterion is required. In this present study, the von-Mises yield criterion is applied:

$$\Phi = \left[\frac{3}{2} (S_{ij} - \alpha_{ij}) : (S_{ij} - \alpha_{ij}) \right]^{\frac{1}{2}} - \sigma_c = 0, \quad (1)$$

Where, S_{ij} and α_{ij} are reduced stresses and deviatoric back stress components respectively. The current yield stress, σ_c , can be additively decomposed into an initial yield stress and an isotropic softening stress.

The plastic modulus is formulated from the consistency condition conforming associative flow rule, incorporating the hardening laws as:

$$h = n_{ij} : \frac{dS_{ij}}{d\varepsilon_{eq}^p} = n_{ij} : \frac{d\alpha_{ij}}{d\varepsilon_{eq}^p} + \frac{d\sigma_c}{d\varepsilon_{eq}^p}, \quad (2)$$

where n_{ij} is the flow vector, and $d\varepsilon_{eq}^p$ is the equivalent plastic strain rate. Here n_{ij} is defined as:

$$n_{ij} = \frac{3}{2} \frac{S_{ij} - \alpha_{ij}}{\sigma_{eq}}, \quad (3)$$

Where σ_{eq} is the von-Mises equivalent stress and where the magnitude of the equivalent plastic strain rate is estimated as,

$$d\varepsilon_{eq}^p = \left[\frac{2}{3} d\varepsilon_{ij}^p : d\varepsilon_{ij}^p \right]^{\frac{1}{2}}. \quad (4)$$

Calculation of plastic modulus, h requires incorporation of hardening rules, the selection of which is very important for the model. The KH law selected for the developing the model is a six-segmented ($m = 6$) Ohno-Wang law [5]. The Masing behaviour of the material for the considered strain range is modelled by a single cyclic yield stress and one set of KH parameters. The total contribution of the six deviatoric back stress segments is:

$$\alpha_{ij} = \sum_{k=1}^m \alpha_{ij}^k. \quad (5)$$

Here, α_{ij}^k is the k^{th} segment of the (deviatoric) back stress tensor, and for each segment, the back stress evolution law is as follows:

$$d\alpha_{ij}^k = \sqrt{\frac{3}{2}} C^k r^k \left[n_{ij} - \left(\frac{\|\alpha_{ij}^k\|}{r^k} \right)^{\chi^k + 1} l_{ij}^k \right] d\varepsilon_{eq}^p. \quad (6)$$

In the above expression, l_{ij}^k is the direction of the corresponding back stress:

$$l_{ij}^k = \frac{\alpha_{ij}^k}{\|\alpha_{ij}^k\|} \quad \text{and}, \quad \|\alpha_{ij}^k\| = \left[\frac{3}{2} \alpha_{ij}^k : \alpha_{ij}^k \right]^{\frac{1}{2}}. \quad (7)$$

C^k , and r^k are the material parameters for the KH law, where C^k are the hardening coefficients and r^k are the saturation values of α_{ij}^k for the k^{th} segment.

4.1. Softening Model (Isotropic):

Recovery or softening by annihilation is always isotropic. The chosen scheme is to calculate the softening stress (negative) σ_2 and algebraically add this to the initial stress to determine the current yield stress, i.e.,

$$\sigma_c = \sigma_0 + \sigma_2. \quad (8)$$

The cyclic softening stress σ_2 is calculated [6] from the dislocation annihilation model [2] at the low angle grain boundaries. This is not discussed in this article. The softening stress is calculated in an incremental form as:

$$\Delta\sigma_2 = -\frac{\alpha M^2 G b}{S_n} \frac{\Lambda}{D} \lambda \frac{y_e}{b} \Delta\varepsilon^p, \quad (9)$$

where α is the interaction strength, M is the Taylor factor, G is the shear modulus, b is the magnitude of the Burger's vector, λ is the dislocation density of edge dislocations at sub-grain boundaries per unit length, D is the average sub-grain size, λ is the slip band width, S_n is the number of independent slip systems (taken to be five to accommodate von-Mises plasticity), and y_e is the critical annihilation distance. If n is the number of annihilation sites per slip band interacting with low angle sub-grain boundaries then, $y_e = \lambda/2n$. If p is the probability of annihilation of dislocations of opposite sign, finally, the plastic modulus is formulated as:

$$h = \sum_{k=1}^m C^k r^k \left[1 - \left(\frac{|\alpha_{ij}^k|}{r^k} \right)^{\lambda^k + 1} l_{ij}^k : n_{ij} \right] - \frac{\alpha M^2 G b p}{S_n} \frac{\Lambda}{D} \frac{\lambda^2}{2nb}. \quad (10)$$

4.2. Ratcheting Model

It is observed after examination of the TEM micrographs of both ratcheted and LCF samples that dislocation sub-cell formation is usually delayed in case of ratcheting. The delay occurs due to a continuous generation dislocations due to asymmetry in loading. Experimental evidence shows that the dislocation density in this material can be fitted using an exponential growth model, hence from the Orowan equation, the increase in dislocation density is derived by Mecking and Kocks [7] as:

$$d\rho = \frac{M}{bL} \frac{dq}{L} - \frac{2y_e \rho M}{b S_n} \frac{dq}{L}, \quad (11)$$

where dq is the increase of the size of the plastic strain memory surface. Chaboche, Dang Van and Cordier [8] have introduced the plastic strain memory surface in strain space where it is given as:

$$F = \frac{2}{3} (\varepsilon_{ij}^p - \beta_{ij}) : (\varepsilon_{ij}^p - \beta_{ij}) - q^2 \leq 0. \quad (12)$$

Here, β_{ij} is the centre of the memory surface and q is the radius. For strain controlled LCF, $\beta_{ij}=0$ and q is a constant equal to the plastic strain amplitude. Therefore, dq is zero. For ratcheting, the plastic strain centre shifts due to the ratcheting strain and thereby the radius of the plastic strain memory surface increases. Chobache et. al. [8] introduced an expression to account for the increase in the size of the plastic strain memory surface, and later McDowell [9] modified the expression adding a threshold term, defined as:

$$dq = \left[\eta H(F) - \xi q (1 - H(F)) \right] \langle n_{ij} : n_{ij}^* \rangle d\varepsilon_{eq}^p. \quad (13)$$

Here, $H(F)$ stands for a heavy side function, n_{ij} is the flow direction, and n_{ij}^* is the normal to the plastic strain memory surface is given as:

$$n_{ij}^* = \frac{2}{3} \frac{\varepsilon_{ij}^p - \beta_{ij}}{q}, \quad (14)$$

where η and ξ are tuning parameters. In this analysis, dq is considered as the measure of the ratcheting strain.

A function, defined by the dislocation density, is employed to control the intensity of hardening by modifying the r^k values of the Ohno-Wang KH law, motivated by the fact that with time, randomly distributed newly generated dislocations are susceptible to pile-up. The function is as follows:

$$f = 1 - \exp \left(- \frac{\rho - \rho_c}{\rho_c} \right). \quad (15)$$

There is a critical density of dislocations (ρ_c) corresponding to the first quarter cycle of the LCF loading, beyond which the unbalanced loading effect come into play. The critical dislocation density acts like a threshold for entry into the ratcheting domain. The function f acts like a scaling function, which operates between 0 to 1 denoting initial and saturated values of r^k respectively. According the r^k values are modified as:

$$r^k = r^k \{1 + (\bar{\chi} - 1)f\}. \quad (16)$$

The evolution of r^k values, shown above, is actually controlled by the function f and the parameter $\bar{\chi}$. The rate of hardening is modulated by the function f and the amount of hardening is governed by the parameter $\bar{\chi}$. For each segment of the KH rule the function and the parameter are kept unchanged for simplicity. The evolution of $\bar{\chi}$ with plastic strain amplitude is assumed to be exponential:

$$\bar{\chi} = \chi_0 + \chi_{sat} \{1 - \exp(-Bq)\}. \quad (17)$$

From the experimental observations, χ_0 and χ_{sat} are determined. χ_0 is taken as 1 to ensure the LCF phenomena in balanced loading where no change in r^k occurs. Within the critical dislocation density no evolution of r^k is allowed. Beyond the critical point, r^k evolve up to a saturation value of χ_{sat} . The values of χ_{sat} and the rate parameter B is found from the secondary ratcheting loops, and calibrated by trial and error.

5. Determination of Material Parameters

The required elastic parameters for the model (shown in table 2) are extracted from the uniaxial tensile tests following standard procedures. The cyclic yield stresses are extracted from the stress-plastic strain data of the uniaxial LCF tests for all strain amplitudes. The variation of yield stresses with strain amplitude is negligible due to the Masing behaviour of the material (figure 5c). The initial cyclic yield stress is found to be 195MPa.

As input to the Ohno-Wang KH Law, the parameters C^k , r^k are determined from the experimental results of uniaxial tension-compression and symmetric cyclic loading at (the highest) strain amplitude of 0.75%. The loading branch of the saturated stress-plastic strain hysteresis loop is divided in six segments ($k = 1, 2 \dots 6$) to obtain one set of the KH parameters. It is evident from experimental results that the material shows the Masing behavior in the plastic strain range of the present work. Therefore, one set of value for C^k and r^k ($k = 1, 2 \dots 6$) can accurately evaluate the kinematic hardening property of the material. The procedure, outlined in the work of Jiang and Kurath [10], has been followed to determine the KH Parameters. The values of C^k and r^k determined for the present material are shown in table 3. Table 4 below provides the estimated values for the cyclic softening parameters. Some of the material parameters are determined from TEM observations and a few are obtained by calibration.

Table 2. parameters of SA333 C-Mn steel, used in simulations.

Young's modulus (GPa)	Poisson's Ratio
207	0.3

Table 3. C^k and r^k values.

$C^1 = 16329.93$	$C^2 = 4082.48$	$C^3 = 1632.99$	$C^4 = 816.49$	$C^5 = 326.59$	$C^6 = 116.64$
$r^1 = 11.77\text{MPa}$	$r^2 = 17.20\text{MPa}$	$r^3 = 21.01\text{MPa}$	$r^4 = 26.14\text{MPa}$	$r^5 = 34.57\text{MPa}$	$r^6 = 36.68\text{MPa}$

Table 4. Material parameter for dislocation annihilation at tilt boundary.

Parameter	α	M	G	b	D	Λ_0	λ	n (per λ)	S_n
Unit			MPa	nm	μm	m^{-1}	nm		
Strain Amplitudes	0.35%	0.30	2.99	80769	0.25	1.2	1.0×10^9	30	13.5
	0.50%								33
	0.75%								90

The evolution of the dislocation density is governed by equation (11). All necessary additionally required material parameters are listed in table 5. The value of the initial dislocation density is taken from literature, and the critical dislocation density (ρ_c) is back-calculated from the evolution law at the quarter cycle, subject to the corresponding symmetric loading amplitude. The values of χ_0 , χ_{sat} and B are fitting parameters, chosen by trial and error.

Table 5. Material parameter for ratcheting model.

Plastic strain amplitude at quarter cycle	L μm	ρ_0 m^{-2}	ρ_c m^{-2}	χ_0	χ_{sat}	B
0.304%	22	1E8	1.5E12	1	0.7	133
0.640%			3.2E12			
1.059%			5.3E12			

6. Finite element simulation

The LCF tests were simulated using the ABAQUS software. Only the working (gauge length) portion of the actual specimens were modelled. Figure 7 shows schematic representation of the model mesh.

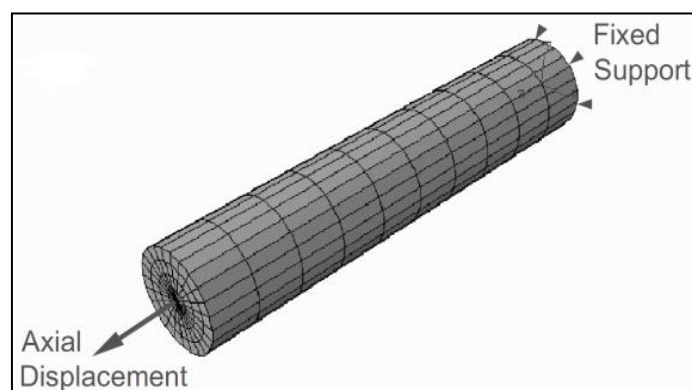


Figure 7. Mesh and loading arrangement for the finite element simulations.

The model for the specimen gauge is discretized using structural meshing. A total of 576 8-noded linear hexahedral elements along with a central zone of 144 6-noded linear wedge elements are used to maintain the radial orientation. For LCF loading, a displacement boundary condition is imposed according to the strain amplitudes using a balanced triangular amplitude function. For ratcheting, a point load corresponding to the peak stress is applied to a reference point connected to the body through kinematic coupling, and an asymmetric triangular amplitude function is employed. The material model is incorporated in the finite element analysis through the user material subroutine (UMAT) with a proper numerical integration scheme.

7. Results and discussion

7.1. Uniaxial low cycle fatigue – validation of the KH rule and softening model

Figure 8 shows a comparison of the experimental and simulated stress-strain hysteresis loops at the 30th cycle, as well as the form of the cycle-dependent softening of the peak stress for tension-compression cyclic loading subject to a strain amplitude of 0.35%.

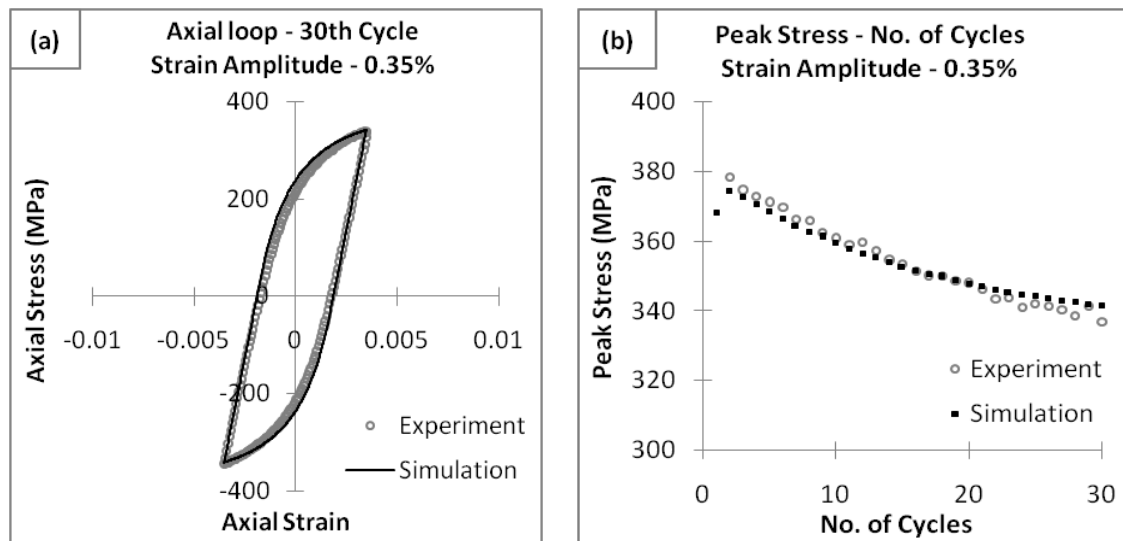


Figure 8. Comparison of uniaxial experimental and simulated results for 0.35% strain amplitude, (a) stress-strain hysteresis loops at 30th cycle, (b) peak stress vs. number of cycles.

7.2. Uniaxial ratcheting loading – validation of the ratcheting model

Qualitative and quantitative matching of both the hysteresis loops and the cyclic softening curvature assures the transferability of the model and necessary material parameters to complex loading conditions such as asymmetric ratcheting loading. Figure 9a-b shows a graphical representation of ratcheting experiments and simulated curves. It is observed that, the ratcheting strain increases with increasing mean stress and increasing stress amplitude. However, for higher stress values (both mean stress and stress amplitude) the model over-estimates the experimental results. Note that the influences of mean stress and stress amplitude are captured separately in the simulation.

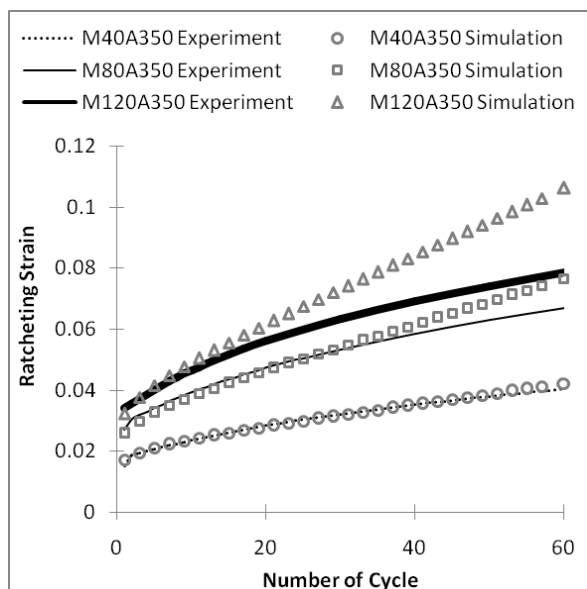


Figure 9a. Constant Stress Amplitude = 350MPa

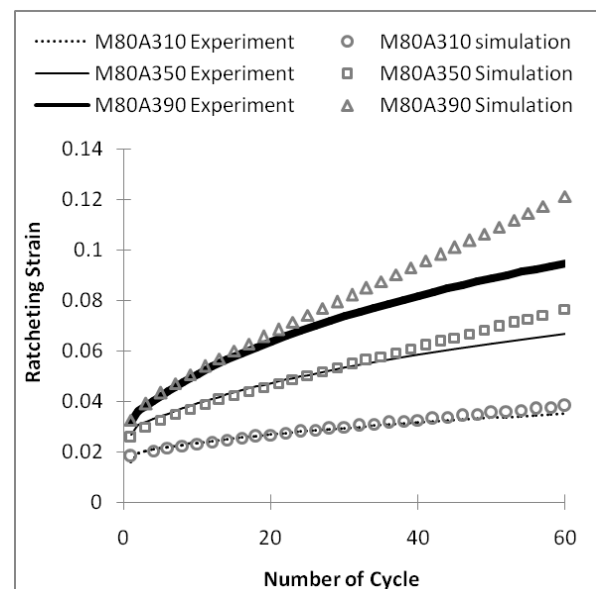


Figure 9b. Constant Mean Stress = 80MPa

8. Conclusion

The present work has examined four cyclic plastic phenomena, namely: i) steady-state hysteresis loops and the Bauschinger effect, ii) the Masing phenomena, iii) cyclic softening in initial transient cycles and, iv) ratcheting. The hysteresis loop shape and Bauschinger effect is well modelled by the Ohno-Wang kinematic hardening law. The parameters for the Ohno-Wang law have been calculated from experimental data on uniaxial LCF loading. It is found that for the material examined (SA333 Grade-6 C-Mn steel) one set of KH parameters is sufficient as the material shows Masing behaviour. Cyclic softening is effectively simulated using model assuming dislocation annihilation at low angle sub-grain boundaries. The ratcheting is simulated by modifying the kinematic hardening contribution by an additional increase in dislocation density due to the asymmetry in loading. Phenomenological modelling results using this model for cyclic softening and ratcheting show a reasonable agreement with the experimental results.

Acknowledgements

The authors acknowledge Bhabha Atomic Research Centre, Mumbai for financial assistance through collaborative project and National Metallurgical Laboratory, Jamshedpur for experimental support. The authors also acknowledge Dr. Surajit Kumar Paul, National Metallurgical Laboratory, Jamshedpur for TEM micrographs.

References

- [1] Read W T and Shockley W 1950 *Physical Review* **78** 3 275
- [2] Sauzay M, Brillet H, Monnet I, Mottot M, Barcelo F, Fournier B and Pineau A 2005 *Materials Science and Engineering A* **400-401** 241
- [3] Cailletaud G and Sai K 2008 *Materials Science and Engineering A* **480** 1–2 24
- [4] Taleb Lakhdar and Hauet Annie 2009 *International Journal of Plasticity* **25** 71359
- [5] Ohno N and Wang J D 1993 *International Journal of Plasticity* **9** 3375
- [6] Sinclair CW, Poole W J and Bréchet Y 2006 *Scripta Materialia* **55** 8739
- [7] Meckings H and Kocks U F 1981 *Acta Metallurgica* **29** 1865
- [8] Chaboche J L, Dang Van K and Cordier G 1979 *SMiRT-5*, Berlin
- [9] McDowell D L 1985 *Journal of Applied Mechanics* **52** 298
- [10] Jiang Y and Kurath P 1995 *International Journal of Plasticity* **12** 3387